

2008

Swimming Dynamics and Propulsive Efficiency of Squids Throughout Ontogeny

Ian K. Bartol

Old Dominion University, ibartol@odu.edu

Paul S. Krueger

Joseph T. Thompson

William J. Stewart

Old Dominion University

Follow this and additional works at: https://digitalcommons.odu.edu/biology_fac_pubs

 Part of the [Biomechanics Commons](#), [Integrative Biology Commons](#), [Marine Biology Commons](#), and the [Zoology Commons](#)

Repository Citation

Bartol, Ian K.; Krueger, Paul S.; Thompson, Joseph T.; and Stewart, William J., "Swimming Dynamics and Propulsive Efficiency of Squids Throughout Ontogeny" (2008). *Biological Sciences Faculty Publications*. 289.

https://digitalcommons.odu.edu/biology_fac_pubs/289

Original Publication Citation

Bartol, I. K., Krueger, P. S., Thompson, J. T., & Stewart, W. J. (2008). Swimming dynamics and propulsive efficiency of squids throughout ontogeny. *Integrative and Comparative Biology*, 48(6), 720-733. doi:10.1093/icb/icn043

Swimming dynamics and propulsive efficiency of squids throughout ontogeny

Ian K. Bartol,^{1,*} Paul S. Krueger,[†] Joseph T. Thompson[‡] and William J. Stewart*

*Department of Biological Sciences, Old Dominion University, Norfolk, VA 23529, USA; [†]Department of Mechanical Engineering, Southern Methodist University, Dallas, TX 75275, USA; [‡]Department of Biology, Franklin and Marshall College, Lancaster, PA 17604, USA

Synopsis Squids encounter vastly different flow regimes throughout ontogeny as they undergo critical morphological changes to their two locomotive systems: the fins and jet. Squid hatchlings (paralarvae) operate at low and intermediate Reynolds numbers (Re) and typically have rounded bodies, small fins, and relatively large funnel apertures, whereas juveniles and adults operate at higher Re and generally have more streamlined bodies, larger fins, and relatively small funnel apertures. These morphological changes and varying flow conditions affect swimming performance in squids. To determine how swimming dynamics and propulsive efficiency change throughout ontogeny, digital particle image velocimetry (DPIV) and kinematic data were collected from an ontogenetic range of long-finned squid *Doryteuthis pealeii* and brief squid *Lolliguncula brevis* swimming in a holding chamber or water tunnel ($Re=20-20\,000$). Jet and fin wake bulk properties were quantified, and propulsive efficiency was computed based on measurements of impulse and excess kinetic energy in the wakes. Paralarvae relied predominantly on a vertically directed, high frequency, low velocity jet as they bobbed up and down in the water column. Although some spherical vortex rings were observed, most paralarval jets consisted of an elongated vortical region of variable length with no clear pinch-off of a vortex ring from the trailing tail component. Compared with paralarvae, juvenile and adult squid exhibited a more diverse range of swimming strategies, involving greater overall locomotive fin reliance and multiple fin and jet wake modes with better defined vortex rings. Despite greater locomotive flexibility, *jet* propulsive efficiency of juveniles/adults was significantly lower than that of paralarvae, even when juvenile/adults employed their highest efficiency jet mode involving the production of periodic isolated vortex rings with each jet pulse. When the fins were considered together with the jet for several juvenile/adult swimming sequences, *overall* propulsive efficiency increased, suggesting that fin contributions are important and should not be overlooked in analyses of the swimming performance of squids. The fins produced significant thrust and consistently had higher propulsive efficiency than did the jet. One particularly important area of future study is the determination of coordinated jet/fin wake modes that have the greatest impact on propulsive efficiency. Although such research would be technically challenging, requiring new, powerful, 3D approaches, it is necessary for a more comprehensive assessment of propulsive efficiency of the squid dual-mode locomotive system.

Introduction

Squids employ a unique dual-mode locomotive system involving both a pulsed jet and movement of the fins. The pulsed jet is formed by first expanding the mantle, a muscular organ that encloses the viscera and the mantle cavity (Fig. 1). As the mantle expands radially, water fills the mantle cavity through intakes at the anterior margin of the mantle. Next, muscles arranged around the circumference of the mantle (i.e., circular muscles) contract. Contraction increases the pressure in the mantle cavity, closes valves on the intake slots, and drives water out of the mantle cavity *via* the funnel, which

can bend within a hemisphere below the body, allowing squids to swim either arms-first or tail-first (Fig. 1). Repetition of these muscle patterns results in a pulsed jet. The fins and funnel, like the mantle, are muscular hydrostats, having densely packed 3D muscular and connective-tissue architectures that permit complex motions without support from bones or fluid-filled cavities (Ward and Wainwright 1972; Kier and Smith 1985; Kier 1988, 1989). The fins of many squids produce waves of bending that travel from the leading to the trailing edge of the fin; the ratio of the length of these waves to the fin chord length varies from low (undulations) to high

From the symposium “Going with the Flow: Ecomorphological Variation across Aquatic Flow Regimes” presented at the annual meeting of the Society for Integrative and Comparative Biology, January 2–6, 2008, at San Antonio, Texas.

¹E-mail: ibartol@odu.edu

Integrative and Comparative Biology, volume 48, number 6, pp. 720–733

doi:10.1093/icb/icn043

Advanced Access publication May 20, 2008

© The Author 2008. Published by Oxford University Press on behalf of the Society for Integrative and Comparative Biology. All rights reserved. For permissions please email: journals.permissions@oxfordjournals.org.

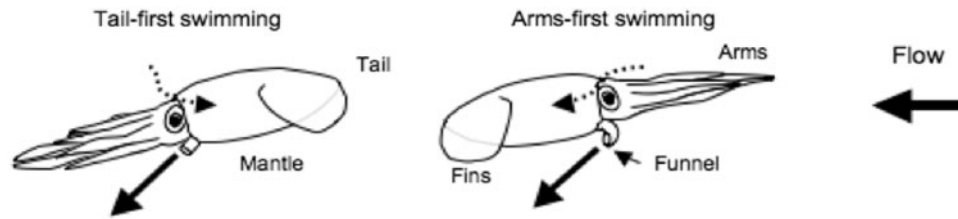


Fig. 1 Illustration of squid swimming in a tail-first and arms-first orientation. Squids swim by flapping/undulating their fins and using a pulsatile jet, while their arms are important for generation of lift and for stability control. The dotted and solid arrows represent the direction of water during mantle refilling and mantle contraction, respectively.

(flaps) values (Hoar et al. 1994; Bartol et al. 2001b; Anderson and DeMont 2005).

The dual-mode propulsive system affords many squids tremendous locomotive flexibility. Using this system, most squids can achieve high levels of maneuverability, having the ability to navigate structurally complex habits, hover, change direction quickly, and even swim almost vertically in the water column. Squids can reach the fastest speeds known among aquatic invertebrates ($\sim 8 \text{ m s}^{-1}$) (Alexander 1977; Vogel 1987), swim arms-first or tail-first (Hanlon et al. 1983; Vecchione and Roper 1991; Bartol et al. 2001a, 2001b), elude predators adeptly (Hanlon and Messenger 1996), and attack fast-moving prey when the system is coupled with rapid-strike tentacles (Kier and van Leeuwen 1997). Some squids, such as the Japanese squid *Todarodes pacificus*, even undergo extensive migrations of 2000 km, during which they swim continuously at an average speed of 0.3 m s^{-1} (Gosline and DeMont 1985).

During ontogeny, squids undergo critical morphological changes that affect their two locomotive systems. Squid paralarvae—a term used for cephalopod hatchlings because they do not undergo a distinct metamorphosis like true larvae but do differ behaviorally, ecologically, and morphologically from adults (Young and Harman 1988; Hanlon and Messenger 1996)—have saccular, rounded bodies and small, rudimentary fins, forcing hatchlings to rely more heavily on the jet than on the fins for propulsion (Boletzky 1974; Okutani 1987; Hoar et al. 1994). Juveniles and adults have more streamlined bodies and larger, more developed fins (Hoar et al. 1994). Although the fins are often overlooked in locomotive studies, the fins play prominent locomotive roles in many juvenile and adult shallow-water squids (Hoar et al. 1994; Bartol et al. 2001a, 2001b; Anderson and DeMont 2005) and are the most important propulsive mechanism for many mesopelagic and bathypelagic squids (Vecchione et al. 2001, 2002). Compared with juvenile and adult squid, paralarvae also have relatively larger funnel apertures (Packard 1969; Boletzky 1974; Thompson and Kier

2002), hold a proportionally greater volume of water in their mantle cavities (Gilly et al. 1991; Preuss et al. 1997; Thompson and Kier 2001a), and have shorter thick filaments in the mantle muscles that provide power for jetting (Thompson and Kier 2006).

As squids undergo morphological changes throughout development, they also experience very different flow regimes. Paralarval forms of *Illex illecebrosus*, *Sepioteuthis lessoniana*, and *Lolliguncula brevis* operate at Reynolds numbers (Re) of $1\text{--}10^2$ while juveniles and adults operate at Re of $10^3\text{--}10^6$ (O'Dor et al. 1986; O'Dor 1988; Thompson and Kier 2002; Bartol et al. 2001b). The giant squid *Architeuthis* operates over a particularly wide Re range from 1 as a paralarva to 10^8 as an adult. Over the wide Re range of squids, the physics of fluids plays an important role in shaping swimming performance. Within the intermediate Re range of paralarvae, both inertia and viscosity have similar relative effects on flow. As a result of the prominent role of viscosity at these Re , continuous swimming is more advantageous than burst-and-coast swimming (Weihs 1974). Rapid jetting in paralarvae resembles burst-and-coast swimming since there is a burst of thrust as the mantle contracts and water is expelled, followed by a coasting phase as the mantle refills. Consequently, more frequent contractions with less coasting presumably should be favored in hatchlings. This prediction is consistent with Thompson's and Kier's (2001a) finding that paralarvae [5 mm dorsal mantle length (DML)] have higher contraction rates of the mantle during escape than do juvenile and sub-adult (10–65 mm DML) oval squid *S. lessoniana*.

The interplay of morphology and fluid mechanics during ontogeny in squids clearly affects swimming performance and propulsive efficiency. Few studies, however, have examined swimming performance and propulsive efficiency over multiple life-history stages in squids. Using kinematic data, morphological measurements, and flow visualization data, Bartol et al. (2001b) made predictions of the relative contributions to force by the fins and jet and of jet propulsive efficiency for a size range of *L. brevis*

from 1.8 to 8.9 cm DML. Thompson and Kier (2002) examined the mechanics of the mantle in *S. lessoniana* (5–40 mm DML) during escape jetting and made predictions of jet propulsive efficiency, based on kinematic and force-transducer measurements. However, neither study involved the global quantification of fluid structure of the jet or fins.

The common measure of propulsive efficiency for jet-propelled organisms is Froude efficiency (Vogel 1994), which takes into account velocity upstream of the jet/propeller and velocity downstream of the jet/propeller (Prandtl 1952). Anderson and DeMont (2000) and Anderson and Grosenbaugh (2005), who examined adult *Doryteuthis pealeii* (formerly *Loligo pealeii*, see Vecchione et al. 2005) (~27 cm DML), suggested using rocket motor propulsive efficiency or whole-cycle propulsive efficiency because they are presumably better suited for squid propulsion. Although all of these equations provide useful information about efficiency, they use theoretical models for thrust and kinetic energy and do not rely on direct measurements of these quantities from bulk properties of the wake (e.g., impulse, kinetic energy, and circulation). Moreover, these equations do not account for unsteady effects that affect calculations of thrust and energy, such as increased exit over-pressure and time-varying, nonuniform velocity profiles, and they have not been applied to the contributions from the fins.

In this article, we examine the dynamics of the jet, and wherever possible, the fins of squid throughout ontogeny using DPIV, and we measure propulsive efficiency using bulk properties (i.e., physical properties such as vorticity, impulse, and kinetic energy) derived from the wakes of the jet and fins. Our approach to propulsive efficiency incorporates direct measurements of wake flows produced by the squid, which distinguishes it from more theoretical approaches to efficiency. Anderson and Grosenbaugh (2005) introduced a similar DPIV-derived approach for the study of jet efficiency in adult *D. pealeii* that involves some measures of momentum and kinetic energy in the wake, but we extend the approach to the study of an ontogenetic range of squids with different swimming strategies. As mentioned above, fins have been largely ignored in previous assessments of performance and of propulsive efficiency despite their being an important locomotive component of many squids. Although we will focus largely on jet dynamics for this paper because jet data are more readily available, we will also discuss the importance of the fins, incorporate fin data into some propulsive efficiency estimates,

and discuss methods of incorporating contributions by fins in future propulsive efficiency research.

Materials and methods

Animal collection and maintenance

Although brief squid *L. brevis* was the target organism for this study, it was not possible to obtain *L. brevis* hatchlings and thus *D. pealeii* paralarvae were used instead. At the paralarval stage, *D. pealeii* is a reasonable surrogate for *L. brevis* because it has similar body size, fin size and shape, and relative funnel diameter. *L. brevis* ranged in size from 2.0 to 8.5 cm DML while *D. pealeii* paralarvae were 0.18 cm DML. *Doryteuthis pealeii* eggs were purchased from the Marine Biological Laboratory, Woods Hole, MA, and maintained in a recirculating seawater system at a salinity of 30–32‰ and at temperatures of 16–19°C until hatching. *L. brevis* were captured by otter trawl within embayments near Wachapreague, VA and maintained in a recirculating seawater system with a salinity of 30–34‰ and temperatures of 19–24°C, using protocols described by Hanlon et al. (1983). *Lolliguncula brevis* were fed a diet of *Palaemonetes pugio* and *Fundulus* spp. and allowed to acclimate for at least 48 h before experimentation.

DPIV Experiments

Doryteuthis pealeii paralarval experiments were conducted in a holding chamber ($4.0 \times 6.0 \times 2.5 \text{ cm}^3$) filled with stationary seawater seeded with neutrally buoyant, silver coated, hollow glass spheres (mean diameter = 14 μm , Potters Industries, Inc., Valley Forge, PA, USA). *Lolliguncula brevis* juvenile/adult experiments were conducted in a 250 l water tunnel (Model 502{S}, Engineering Laboratory Design, Inc., Lake City, MN, USA) with a $15 \times 15 \times 43 \text{ cm}^3$ working section filled with the same tracer particles. *Doryteuthis pealeii* were allowed to acclimate for 5 min prior to experimentation. *Lolliguncula brevis* were allowed to acclimate to the water tunnel for 15–30 min at a speed setting of 2–4 cm s^{-1} . After acclimation, the water tunnel speed was increased in 1 cm s^{-1} stepwise increments, lasting ~10 min, until the squid could no longer keep pace with free-stream flow. During each 10 min speed increment, DPIV data were collected using protocols described below. One squid was examined in the water tunnel during each *L. brevis* experimental trial. However, to increase the probability of imaging a free-swimming paralarvae within a limited field of view (FOV), 3–6 *D. pealeii* paralarvae were placed in the holding chamber during experimental runs. Although squid

are capable of swimming in both arms-first and tail-first orientations, the tail-first mode was the focus of the current study.

Two pulsed ND: YAG lasers (wavelength = 532 nm; power rating 350 mJ/pulse; LaBest Optronics Co. Ltd., Beijing, China), each operating at 15 Hz (0.07 ns pulse duration) with a 1–4 ms separation between pulses, were used, together with an optical guide arm, to illuminate the light-reflective particles. The particles were illuminated in a 0.5 mm (using an aperture) or 1–2 mm thick parasagittal plane for paralarval and juvenile/adult experiments, respectively. In all experiments a UNIQ UP-1830CL 8 bit “double-shot” video camera (1024 × 1024 pixel² resolution; paired images collected at 15 Hz; Uniq Vison, Inc., Santa Clara, CA, USA) interfaced with a CL-160 capture card (IO industries, Inc., London, Ontario, Canada) was used. The camera was positioned orthogonally to the laser plane to record movements of particles around the squid. A VZM 450i zoom lens (Edmund Optics, Barrington, NJ, USA) was used in paralarval experiments to image flows for FOVs ranging from 0.8 × 0.8 to 2.0 × 2.0 cm², while a Computar 12–36 mm lens was used in juvenile/adult experiments to image flows for FOVs ranging from 8 × 8 to 14 × 14 cm². Fine-scale focusing and movement of the cameras were achieved using a series of optical stages (Optosigma, Santa Ana, CA, USA).

In addition to the UNIQ UP-1830CL camera, two high-speed DALSA IM150 video cameras (1024 × 1024 pixel² resolution; frame rate set at 100 Hz; DALSA Corp., Waterloo, ON) outfitted with Fujinon CF25HA-1 25 mm lenses were used to record motions of the body and fins, both for paralarval and juvenile/adult experiments. One camera was positioned underneath the working section to record images from a ventral perspective and the other was positioned directly beside the UNIQ camera for an expanded lateral FOV of the squid. Because the UNIQ and DALSA cameras were operated at different frame rates, separate lighting, and spectral filters were used, depending on the camera. A series of four 40 W lights outfitted with a color gel #27 filter (transmits wavelengths >600 nm Rosco Laboratories, Inc., Stamford, CT, USA) provided illumination for the high-speed DALSA cameras, while the laser light (532 nm) provided the illumination for the DPIV UNIQ camera. A Kodak Wratten 32 magenta filter (blocks wavelengths 520–600 nm) was mounted to the DALSA camera lenses to prevent overexposure of laser light, and an IR filter and a Kodak Wratten 58 green filter (transmits wavelengths of 410–600 nm) were mounted to the UNIQ UP-1830CL camera lens to prevent overexposure from the 40 W halogen lights.

The lasers and DPIV camera were triggered and synchronized using a timing program developed by the Gharib lab (California Institute of Technology, Pasadena, CA, USA), a PCI-6602 counter/timing card (National Instruments, Inc., Austin, TX, USA), and a BNC-565 pulse generator (Berkeley Nucleonics Corp., San Rafael, CA, USA). A 4003A signal generator (B&K Precision Corp., Yorba Linda, CA, USA) was used to trigger the DALSA cameras at 100 Hz. All cameras and the optical laser arm were mounted on a four-axis traverse system (Techno-Isel, New Hyde Park, NY, USA). Using a joystick, a PCI-7344 motion controller board (National Instruments), and a LabVIEW VI (National Instruments, Inc., Austin, TX, USA), the three cameras and laser arm were moved simultaneously along the traverse to follow the target squid to different areas of the water tunnel/holding chamber and reposition the laser sheet to bisect either the funnel or fin. To avoid inaccurate flow measurements, data were only collected when the cameras and laser arm were stationary.

For analysis of the DPIV data, each image was subdivided into a matrix of 32 × 32 pixel² interrogation windows. Using a 16 pixel offset (50% overlap), cross-correlation was used to determine the particle displacements within interrogation windows comprising the paired images using *PixelFlow*TM software (FG Group LLC, San Marino, CA, USA) (Willert and Gharib 1991). Outliers, defined as particle shifts that were three pixels greater than their neighbors, were removed and the data were subsequently smoothed to remove high frequency fluctuations. Window shifting was performed followed by a second iteration of outlier removal and smoothing (Westerwheel et al. 1997). Using *PixelFlow*TM software, velocity vector and vorticity contour fields were determined.

Kinematic measurements

Mantle contraction and refill periods, maximum funnel diameter (D) during the jet cycle, fin upstroke and downstroke periods, displacement during contraction and refilling, and frame-by-frame swimming speeds were measured from lateral DPIV/high-speed video footage using the National Institute of Health's public domain program ImageJ (<http://rsb.info.nih.gov/ij/>) and Matlab code written by T Hedrick (University of North Carolina, Chapel Hill, NC; available at <http://www.unc.edu/~thedrick/software1.html>). The mantle and funnel orifice were nicely illuminated in the laser sheet, allowing for precise measurements of the mantle and funnel diameters.

Calculations of impulse, kinetic energy, and propulsive efficiency

Several Matlab (MathWorks, Inc., Natick, MA, USA) utilities were used to calculate hydrodynamic impulse and kinetic energy, all of which assume axisymmetry about the axis of a shed vortex's jet centroid, irrespective of whether the jet was produced by mantle contraction or by the fins. First, the slope and y -intercept of the jet centerline were determined, based on a best fit of the velocity and vorticity data. The length of the jet (L) was the extent of the velocity field along the jet centerline. Second, using the angled centerline as the $r=0$ axis, jet impulse (I) and kinetic energy (E) were computed using the equations:

$$\frac{I}{\rho} = \pi \int_{\text{jet}} \omega_{\theta} r^2 dr dx \quad (1)$$

$$\frac{E}{\rho} = \pi \int_{\text{jet}} V^2 r dr dx \quad (2)$$

where V is the velocity magnitude and ω_{θ} is the azimuthal component of vorticity, r is the radial coordinate, and ρ is the fluid density. The area integrals were computed using a 2D version of the trapezoidal rule. The effects of the velocity field around a vortex (not induced by the vortex itself) were considered to have negligible influence on impulse calculations because all vortices considered in our analysis were spaced more than one ring diameter away from other vortices or boundaries. For juveniles/adults, background flow, i.e., speed of the water in the tunnel, was subtracted from the flow velocity field so that only excess kinetic energy was measured. Third, the components of the impulse vector in the vertical and horizontal directions were computed, based on the slope of the jet centerline relative to the direction of the primary displacement. Because the direction of primary displacement was not aligned along a horizontal axis in paralarvae, as was the case for juveniles/adults, it was necessary to compute a displacement angle using ImageJ. Using this displacement angle and the jet angle determined from the Matlab routine, the component of the impulse aligned with the direction of displacement was computed for paralarvae.

Paralarvae generally do not swim in horizontal paths through the water column as do juvenile and adult squid; instead they swim predominantly upward during mantle contraction and sink during mantle refilling, with net vertical displacement determined largely by the duration of the refill phase. Because work

done by the propulsive system and not work done by gravity is of interest, the effect of gravity on the net motion was factored out by considering only the motion during jet ejection. Therefore, to compare jet propulsive efficiency for paralarvae with that of older life-history stages that swim more horizontally, propulsive efficiency was computed for only the exhalant phase of the jet cycle.

The equation used to calculate jet propulsive efficiency during the exhalant phase of the jet cycle for an ontogenetic range of squid (paralarvae to adults) was:

$$\eta_{P(\text{jet})} = \frac{\tilde{F}_j x}{\tilde{F}_j x + \overline{E}_{EJ}} \quad (3)$$

where \tilde{F}_j = jet thrust time-averaged over the mantle contraction (N), x = displacement during mantle contraction (m), and \overline{E}_{EJ} = total excess kinetic energy of the jet (J). Time-averaged jet thrust, \tilde{F}_j , was determined by dividing the impulse (Ns) component in the direction of displacement by the mantle-contraction period (s). The impulse used in this and all subsequent calculations of propulsive efficiency is the mean of measurements of impulse over several frames after termination of either the jet stroke or the fin stroke; the excess kinetic energy is the peak excess kinetic energy measurement after termination of the jet stroke or fin stroke within the same sequence of frames.

For some swimming sequences of juveniles and adults, where the squid swam well in the laser plane, it was possible to use the rail system to image flows from the jet and fins alternately within a short time window (tens of seconds) while the squid swam at a specific speed. For these sequences, the relative contributions to force by the fins and jet were determined. Time-averaged jet thrust, \overline{F}_j , was determined by dividing the impulse (Ns) component in the direction of displacement by the full jet period (s), i.e., time for contraction and refilling. Time-averaged fin thrust, \overline{F}_f , was computed in several steps. First, time-averaged force contributions were computed separately for fin upstrokes and downstrokes by dividing the impulse (determined from several frames after termination of the fin stroke) from two to five sequential upstrokes or downstrokes by the average duration of the target half-stroke. Second, upstroke and downstroke forces were separated into horizontal and vertical components based on the mean centroid jet angles. Finally, \overline{F}_f was computed by adding the mean horizontal force components of the upstrokes and downstrokes. Since no paralarval fin data were collected because of insufficient spatial

resolution, more conventional propulsive-efficiency equations were used to compare jet and fin efficiency in juveniles and adults. These equations, which were proposed by Lighthill (1960) and incorporate average forces and average kinetic energy, are listed below:

$$\eta_{P(\text{jet})} = \frac{\overline{F}_j U}{\overline{F}_j U + \overline{E}_{Ej}} \quad (4)$$

$$\eta_{P(\text{fins})} = \frac{\overline{F}_f U}{\overline{F}_f U + \overline{E}_{Ef}} \quad (5)$$

where $\eta_{P(\text{jet})}$ = propulsive efficiency of jet, $\eta_{P(\text{fins})}$ = propulsive efficiency of fins, \overline{F}_j = time-averaged jet thrust, \overline{F}_f = time-averaged fin thrust, U = swimming speed, \overline{E}_{Ej} = rate of excess kinetic energy shed by the jet, and \overline{E}_{Ef} = rate of excess kinetic energy shed by the fins. To determine how propulsive efficiency based on both the jet and fins compares to propulsive efficiency based on only the jet, an overall propulsive efficiency, $\eta_{P(\text{Overall})}$, was computed using:

$$\eta_{P(\text{Overall})} = \frac{(\overline{F}_j + \overline{F}_f) U}{(\overline{F}_j + \overline{F}_f) U + \overline{E}_{Ej} + \overline{E}_{Ef}} \quad (6)$$

Results

Jetting and finning at intermediate Re

Doryteuthis pealeii paralarvae spent the majority of their time holding station in the water column; they ascended during mantle contraction and descended during mantle refilling. The duration of the refill period largely determined net vertical displacement in the water column. A total of 20 paralarval swimming sequences, none of which involved paralarvae swimming near the water surface or holding chamber walls, were considered for this study. During these

sequences, the mean peak swimming velocity was $2.67 \pm 1.02 \text{ cm s}^{-1}$ (SD) [$14.83 \pm 5.67 \text{ DML s}^{-1}$ (SD)] with a range of $1.62\text{--}4.84 \text{ cm s}^{-1}$ ($9.0\text{--}26.89 \text{ DML s}^{-1}$). The mean funnel angle (relative to horizontal) of the jets in these sequences was $82.6 \pm 8.0^\circ$ (SD) with a range of $35.4\text{--}89.2^\circ$. Although some spherical vortex rings were observed (Fig. 2A), most jets consisted of an elongated vortical region of variable length (Fig. 2B). In Fig. 2B, the measured vorticity may represent a vortex ring/trailing jet complex [analogous to that observed by Gharib et al. (1998)] where viscous diffusion has blurred the separation between the ring and jet so that “pinch-off” is not readily apparent. Alternatively, the measured vorticity may represent a vortex ring whose formation (i.e., shear layer roll-up) was preempted by viscous diffusion so that a vortical “tail” remains behind the ring. It was not possible to distinguish between these two cases based on our measurements. Therefore, the term “elongated vortex ring” is used here to describe flows, such as those observed in Fig. 2B for paralarval swimming, where the vortex structure has a higher aspect ratio than that commonly called a “vortex ring” or “vortex ring puff” but it has a shorter aspect ratio than does the more prolonged emission of fluid generally associated with a jet. “Elongated vortex ring” is a qualitative descriptor and is not intended to be mathematically or physically rigorous. The mean ratio of jet plug length (L) (based on the velocity field extent) to funnel diameter (D) was 21.8 ± 8.1 (SD) with a range of $14.4\text{--}49.2$. The mean mantle contraction period was $0.095 \pm 0.02 \text{ s}$ (SD) and the mean ratio of peak jet velocity to swimming velocity was 1.14 ± 0.41 (SD), with some peak jet velocities being less than the swimming velocity.

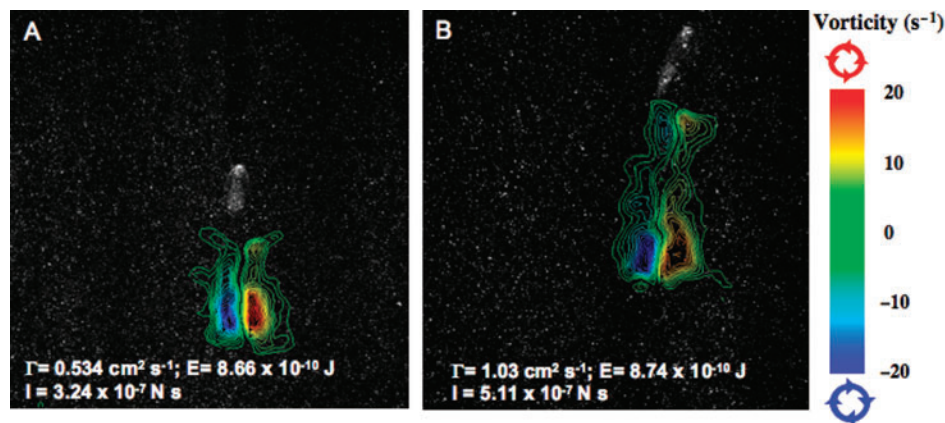


Fig. 2 Vorticity contour fields for a paralarval *D. pealeii* swimming at (A) 3.09 cm s^{-1} (17.2 DML s^{-1}) ($L/D = 24.4$) and (B) 4.84 cm s^{-1} (26.8 DML s^{-1}) ($L/D = 26.1$). Red and blue regions denote counterclockwise and clockwise rotation, respectively. Γ = circulation; E = kinetic energy; I = impulse.

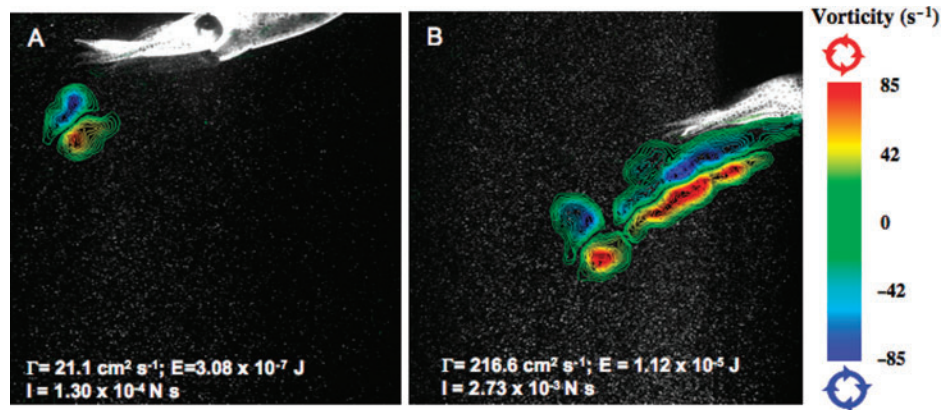


Fig. 3 Vorticity contour plots of the jet of a 4.2 cm DML *L. brevis* swimming at 6 cm s^{-1} (1.43 DML s^{-1}) ($L/D = 6.2$) (A) and a 6.2 cm DML *L. brevis* swimming at 10 cm s^{-1} (1.61 DML s^{-1}) ($L/D = 19.6$) (B). (A) illustrates *jet mode I* and (B) illustrates *jet mode II*. Red and blue regions denote counterclockwise and clockwise rotation, respectively. Γ = circulation; E = kinetic energy; I = impulse.

During most swimming sequences, one fin downstroke coincided with each mantle contraction. During refilling, the fins were held fully extended, thereby probably reducing sinking rate. Our experimental set-up did not have sufficient spatial resolution to resolve fin flows. However, production of force by the fins was probably very low relative to that by the jet; during several refill periods, the fins were actively beating but the body continued to sink rapidly until the onset of the next jet pulse.

Jetting and finning at high Re

A total of 50 jet sequences from juvenile/adult *L. brevis* ranging in size from 2.0 to 8.5 cm DML and swimming over a range of speeds from 2.4 to 18.6 cm s^{-1} (0.8 – 3.2 DML s^{-1}) were considered for this study. Within these sequences a wide diversity of jet patterns were observed. However, two principal hydrodynamic jet modes emerged: (1) a slow swimming mode in which the ejected fluid rolled up into an isolated vortex ring with each jet pulse (*jet mode I*) and (2) a fast swimming mode in which a leading vortex ring pinched off from a long trailing jet during each jet pulse (*jet mode II*) (Fig. 3). Although both modes were observed in all post-paralarval life-history stages, *jet mode I* was most often observed at low speeds and for earlier ontogenetic stages. The mean L/D ratio for *jet mode I* was 5.78 ± 1.81 (SD) with a range of 3.87 – 7.84 . The mean L/D ratio for *jet mode II* was 12.13 ± 4.66 (SD) with a range of 6.97 – 20 . Over the speed range considered, jet angle decreased with increased swimming speed for all juvenile/adult *L. brevis*, with angles relative to horizontal ranging from 16.5° (high speeds) to 57.3° (low speeds). The mean contraction period was $0.25 \pm 0.05 \text{ s}$ (SD) and the mean ratio of

peak jet velocity to swimming velocity was 5.18 ± 2.68 (SD).

A smaller size range of juvenile/adult *L. brevis* was considered for DPIV fin analysis (3.5 – 6.2 cm DML). As was the case with jet wake sequences, there was a wide diversity of observed fin wake modes. The two most prevalent wake patterns were: (1) *fin mode I*, in which a vortex ring was shed with each upstroke and downstroke with no apparent interaction between shed vortices and (2) *fin mode II*, in which a more complicated vortex structure was observed with the apparent merging of a downstroke leading edge vortex with the subsequent upstroke trailing edge vortex (Fig. 4). In *fin mode I*, upstroke circulation was generally less than downstroke circulation. *Fin mode I* and *fin mode II* were detected at speed ranges of 0.4 – 1.67 DML s^{-1} and 0.92 – 1.89 DML s^{-1} , respectively. In *fin mode I* the mean jet angles for upstrokes and downstrokes were $43.9 \pm 17.5^\circ$ above and $52.6 \pm 22.8^\circ$ below a horizontal axis, respectively. In *fin mode II* the mean jet angles for upstrokes and downstrokes were $51.7 \pm 13.0^\circ$ above and $43.8 \pm 18.2^\circ$ below a horizontal axis, respectively.

Propulsive efficiency

Three size classes were considered for calculations of propulsive efficiency: (1) paralarvae (0.18 cm DML); (2) juveniles (2.0 – 4.9 cm DML); and (3) adults (5.0 – 8.5 cm DML). No significant difference in propulsive efficiency was detected between the juvenile and adult size ranges (one tailed t -test, $P = 0.433$), and thus they were pooled for comparisons with paralarvae. Paralarvae had significantly higher jet propulsive efficiency than did juveniles/adults (one tailed t -test, $P < 0.001$). Mean paralarval jet propulsive efficiency was $87.4 \pm 6.5\%$ (SD) with a range of 73.5 – 95.8% , whereas juveniles/adults (2.0 – 8.5 cm DML) had

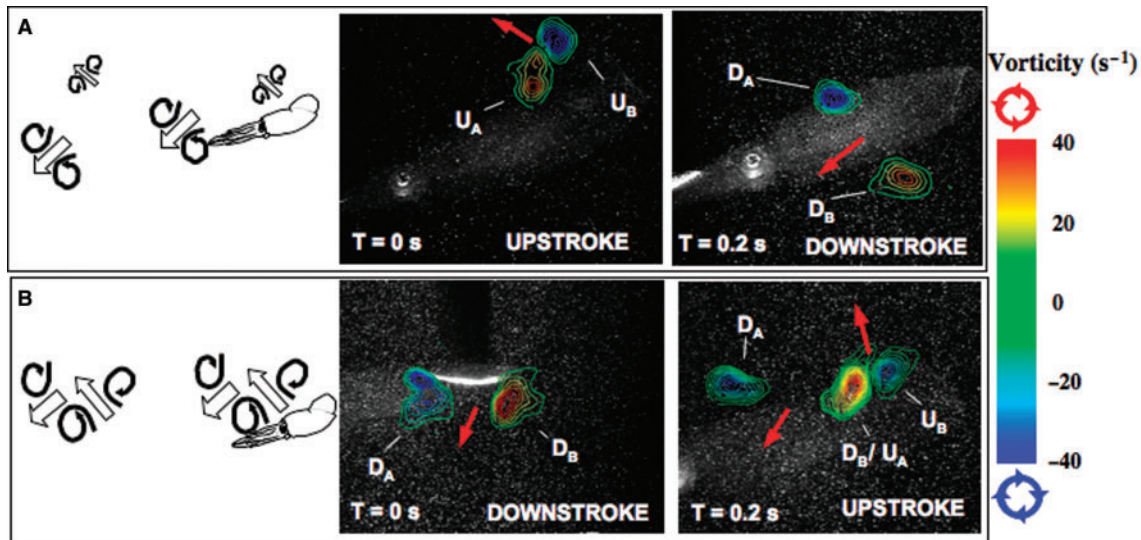


Fig. 4 Schematic drawings and vorticity contour fields of two fin wake modes detected in brief squid *L. brevis* (A = fin mode I; B = fin mode II). Two sequential half strokes are depicted with elapsed time included in the lower left-hand corner. Red arrows denote the direction of vortex ring jets, while red and blue regions denote counterclockwise and clockwise rotation, respectively. U_A = upstroke trailing-edge vortex, U_B = upstroke leading-edge vortex, D_A = downstroke trailing-edge vortex, D_B = downstroke leading-edge vortex, and I = merged vortex complex.

a mean jet propulsive efficiency = $77.8 \pm 11.6\%$ (SD) with a range of 49.4–88.8%. For juveniles and adults, *jet mode I* had a significantly higher jet propulsive efficiency [mean = $80.7 \pm 10.2\%$ (SD)] than did *jet mode II* [mean = $71.3 \pm 13.3\%$ (SD)] (one tailed *t*-test, $P < 0.01$).

Four swimming sequences of juveniles/adults (4.6–6.2 cm DML) involving both fin and jet measurements were examined for swimming speeds ranging from 1.1 to 1.7 DML s^{-1} . These sequences involved both *jet modes I* and *II* but only *fin mode I*. *Fin mode II* was not considered in these analyses because of the difficulties in computing forces from complex, possibly interconnected vortex structures. Relative thrust contributions of the fins and jet varied greatly. The jet contributed 16.8–95.5% of the overall thrust, while the fins contributed 4.5–83.2% of the overall thrust in these sequences. Propulsive efficiency of the fins ranged from 51.5% to 93.0%, and propulsive efficiency of the jet varied from 43.3% to 82.2%. Fin propulsive efficiency [mean = $81.3 \pm 19.8\%$ (SD)] was significantly greater than jet propulsive efficiency [$70.2 \pm 18.5\%$ (SD)] (paired *t*-test: $P < 0.001$). In the four sequences considered, overall propulsive efficiency $\eta_{p(\text{Overall})}$ was 0.8–10.2% greater than jet propulsive efficiency $\eta_{p(\text{jet})}$, and these differences were significant (paired *t*-test: $P = 0.027$). Error in propulsive efficiency due to asymmetry in the vorticity field was determined from differences in the positive and negative vorticity components of the vorticity field and application of standard error

propagation (Holman 2000). Efficiency errors based on this approach ranged from 1.8% to 4.9%.

Discussion

This study demonstrates that paralarvae have different jet dynamics and propulsive efficiencies than do juveniles and adults, which is not surprising given the morphological, fluid mechanical, and ecological shifts these life-history stages experience. Although paralarvae are broadly similar in form to juveniles/adults and do not undergo dramatic alterations in morphology (Boletzky 1974; Sweeney et al. 1992), there are important morphological differences between paralarvae and juveniles/adults. Relative to a juvenile or adult, a paralarva's rudimentary fins are thought to contribute little to production of thrust (Boletzky 1987; Hoar et al. 1994). Our observations of rapid paralarval sinking during mantle refill, even when the fins were active, support this prediction. Thompson and Kier (2006) determined that thick filaments of the mantle muscles that provide power for the jet were 1.5 times longer in juvenile and adult *S. lessoniana* than in paralarvae, and they predicted that this may allow paralarvae to contract their mantles at higher rates than do adults. The *S. lessoniana* paralarvae do indeed exhibit higher contraction frequencies than do adults during escape jetting (Thompson and Kier 2006), and paralarval *D. pealeii* had shorter contraction periods during routine swimming than did adult *L. brevis* in the present study. Paralarvae have larger relative funnel

diameters than do adults (Packard 1969; Boletzky 1974; Thompson and Kier 2002), and some paralarvae, such as *S. lessioniana*, exhibit lower peak mass-specific thrust and higher relative mass flux than do adults during escape jetting (Thompson and Kier 2001a). Based on these findings, Thompson and Kier (2001a) predicted that velocity of expelled water should be lower in paralarvae relative to adults, which again is consistent with findings from the present study.

The unique morphological characteristics of paralarvae (i.e., rudimentary fins, short thick filament lengths in the muscles that provide power for jetting, and relatively large funnel diameters) all have relevance for swimming performance within a hatchling's resident flow regime. After hatching from eggs, paralarvae begin swimming immediately within an intermediate Re regime, where both viscous and inertial forces are important. Since coasting is inhibited in this flow regime, having mantle properties that facilitate higher frequency pulsing and reduced duration of coasting is beneficial for swimming performance. Within the intermediate Re regime, drag-based mechanisms of propulsion can be beneficial (Vogel 2003), but the fins appear to be too rudimentary and small to contribute significantly to undulatory drag-based swimming forces, and thus the highly pulsed jet is the dominant propulsive mechanism. Although jets are thought to be inherently inefficient because they produce thrust by imparting relatively large accelerations to relatively small masses of water (Alexander 1968; Lighthill 1970; Vogel 2003), Thompson and Kier (2001a) found that paralarvae expel relatively large volumes of water through relatively large funnel apertures at low velocities during escape jetting. Consequently, these authors predicted that paralarvae likely enjoy high propulsive efficiency during routine swimming.

Measurements of propulsive efficiency derived from bulk properties of the jet wake in the present study indicate that paralarvae exhibit higher jet propulsive efficiency than do juveniles and adults, and large-volume, relatively low-velocity jets were clearly apparent in the paralarval data (peak jet velocities were $1.14\times$ higher than swimming speed for paralarvae versus $5.15\times$ higher for older life history stages). In fact, in some sequences, the peak jet velocity was less than the swimming speed of the paralarvae. This may be the result of several factors. First, pulsed jet thrust derives from both jet momentum and over-pressure (Krueger and Gharib 2003). Consequently it is plausible that unsteady effects are providing so much over-pressure that only low jet

velocities are needed for the requisite thrust at these low/intermediate Re . Second, the laser sheet width (~ 0.5 mm) was $\sim 25\%$ of ring diameter (~ 2.0 mm), which caused the DPIV measurements to be averaged over the middle 25% of the jet, lowering the measured impulse and kinetic energy values. However, the effects on propulsive efficiency were presumably low given that both impulse and kinetic energy were lowered and our calculations estimate only a 6% reduction in kinetic energy and an 8% reduction in jet centerline velocity due to laser sheet thickness. Third, viscous effects at these low/intermediate Re may dissipate the kinetic energy of the jet and reduce peak velocities when bulk properties of the ring structure are measured after some delay following their formation. To quantify dissipation, regression analyses of kinetic energy on time were performed. Based on the regression slopes and the time delay between the end of the jet (determined from high-speed video frames of mantle and funnel diameters) and the first measurement of kinetic energy (~ 0.02 s), mean dissipation of kinetic energy for paralarvae was $7.8 \pm 4.3\%$ (SD) with a range of 1.3–11.3%. Even if the last two factors led to overestimates of propulsive efficiency and hatchlings actually have similar propulsive efficiencies to juveniles/adults, our findings are nonetheless noteworthy given the vast Re range considered.

One unexpected finding was the shape and high L/D ratio of many of the paralarval jet wakes. Based on engineering studies involving pulsed mechanical jets from rigid tubes, there is a physical limit to the size of a vortex ring. This physical limit occurs when the length of the ejected plug of fluid (L) is $\sim 4\times$ the diameter of the jet aperture (D). This physical limit is known as the formation number (F) (Gharib et al. 1998). Once this limit is reached, vortex rings stop forming midway through the pulse and the remainder of the fluid forms a jet of fluid that trails behind the vortex ring (Gharib et al. 1998) (Figs 2 and 3). At F , the thrust per pulse of a pulsed jet is maximized for a given expelled volume of water (Krueger and Gharib 2003, 2005). L was determined a little differently in mechanical studies than in the present squid study. In mechanical studies, L was the distance a piston pushed a column of fluid in a tube before the fluid exited a nozzle, whereas in the present study, L was the jet length measured from the extent of the velocity field along the jet centerline. The two measurements are similar, but the latter tends to be smaller for $L/D > 1$. Despite this difference in L measurements, L/D s close to four were expected based on the high pulsing rates and large funnel apertures of paralarvae. Instead, elongated

vortex rings with $L/Ds \sim 20$ were most frequently observed as a result of the large volume of water expelled.

The results from the present study indicate that a large-volume, low-velocity jet with a high L/D can lead to high propulsive efficiency, just as shorter-length jets pulsed close to an $L/D = 4$. Anderson and Grosenbaugh (2005) also found this to be the case in adult *D. pealeii*, which produce low-velocity, large-volume, high L/D jets with average propulsive efficiencies as high as 93%. The observation of large volume jets with high L/Ds in both *D. pealeii* paralarvae (0.18 cm DML) and adults (~ 27 cm DML) is intriguing and begs the question: do *D. pealeii* employ different jet strategies throughout ontogeny (elongated rings and longer jets) than *L. brevis* (isolated rings and rings + trailing jets)? Although *D. pealeii* and *L. brevis* hatchlings are similar in size, mantle shape, fin size and shape, and relative funnel diameter, a complete ontogenetic series of both species is required to fully address this important question.

Do higher propulsive efficiencies translate to a lower cost of transport for paralarvae relative to larger life-history stages? The answer to this is probably “no,” but the issue of cost of transport is ambiguous when comparing paralarvae and older life-history stages. First, mass-specific metabolic rates are generally higher in hatchlings than in adults (O’Dor and Webber 1986; O’Dor et al. 1986), which is probably largely attributable to the costs of overcoming relatively high viscous drag forces at low Re . In fact, high-speed kinematic and DPIV data from the present study indicate that half the total paralarval impulse goes towards overcoming drag alone! Second, and perhaps most importantly, paralarvae are largely planktonic as opposed to nektonic as are the juveniles and adults. Paralarvae can certainly reach impressive speeds. *Loligo vulgaris* reach 16 cm s^{-1} (26.7 DML s^{-1}) (Packard 1969); *L. opalescens* paralarvae capture prey at 7.2 cm s^{-1} (24.0 DML s^{-1}) and reach speeds of 12 cm s^{-1} (40.0 DML s^{-1}) during escape jetting (Preuss et al. 1997); *I. illecebrosus* can reach speeds of 5.0 cm s^{-1} (27.8 DML s^{-1}) (O’Dor et al. 1986); and *D. pealeii* can swim at speeds as high as 15 cm s^{-1} (83.3 DML s^{-1}) (J. Thompson, unpublished data). However, paralarvae generally do not reach these speeds while swimming horizontally; they are predominantly vertical, positively phototactic, negatively geotactic migrators that depend heavily on currents for horizontal displacement (Fields 1965; Sidie and Holloway 1999; Zeidberg and Hamner 2002). Some paralarvae, such as those of *L. opalescens*, undergo

daily vertical migrations of 15 m (5000 DMLs!) and remain entrained within cyclonic gyres near shore waters (Zeidberg and Hamner 2002). Older life-history stages are capable of translocating over large distances without the aid of horizontal currents and do not share a similar vertically oriented lifestyle. Because their ecologies are so disparate, comparisons of cost of transport between paralarvae and older life-history stages provide limited insight into the ontogeny of swimming performance.

A key morphological and ecological transition seems to occur at about 1.5 cm DML, when paralarvae become juveniles and swim horizontally against stronger currents (M. Vecchione, R. Hanlon, personal communication). In *S. lessoniana*, maximum amplitude of mantle contraction, hyperinflation, and contraction rate occur in paralarvae during escape jetting; these parameters all decrease as the hatchling grows to a size of 1.5 cm DML then remain unchanged at larger sizes (Thompson and Kier 2001a). This transition in mantle kinematics correlates well with a change in the organization of networks of mantle connective tissue fibers (Thompson and Kier 2001b) but we do not know if it also occurs concurrently with changes in fin, funnel, or mantle mechanics.

According to the results of this study, loliginid squid exhibit greater locomotive flexibility, both in terms of jet and fin dynamics, at sizes >2.0 cm DML. The two principal hydrodynamic jet modes detected in this study (*jet mode I* and *jet mode II*) for juveniles/adults differ from the observed jet wakes of paralarvae. Both of the juvenile/adult jet modes involved well-defined spherical vortex rings, either as the main component of the jet wake (*jet mode I*) or as a leading edge component that detaches from a long trailing jet (*jet mode II*). Although some spherical vortex rings were observed in paralarval jets, most jets consisted of “elongated vortex rings” whereby viscous diffusion either (1) obscured the separation between a leading ring and trailing jet resulting in no clear “pinch-off” or (2) preempted vortex ring formation resulting in the presence of a vortical tail. The presence of well-defined spherical vortex rings in both of the juvenile/adult jet modes is significant because spherical vortex rings accelerate ambient fluid by entrainment and added mass effects, resulting in increased thrust relative to an equivalent steady jet without coherent rings (Krueger and Gharib 2003, 2005). Interestingly, Anderson and Grosenbaugh (2005) mostly observed elongated jets with no discernible or diminished leading vortex rings in larger, adult long-finned squid *Doryteuthis pealei* (DML = 27.1 ± 3.0 cm), with the emitted flow

structure ultimately breaking up into “packets of vorticity of varying degrees of coherence.” Moreover, steady propulsion by individual vortex rings was not observed, suggesting that perhaps larger squids only exhibit *jet mode II* or even another mode with a less well-developed leading edge vortex ring.

Jet mode I is of special significance because the vortex rings presumably occur near the physical limit of vortex-ring formation, i.e., F . As mentioned above, $F \sim 4$ for pulsed mechanical jets in stationary water (Gharib et al. 1998). The L/D s reported in this study for isolated vortex rings were often >4 , reaching values as high as 7.8. F -values as high as eight also have been observed in fast-swimming hydro-medusan jellyfish *Nemopsis bachei* (Dabiri et al. 2005, 2006). The high F -values for biological jetters are not surprising, given that they employ behavioral control of the funnel/aperture opening during ejection (O’Dor 1988; Bartol et al. 2001b; Anderson and DeMont 2005; Dabiri et al. 2006). In experiments involving temporally variable mechanical jet generators, Dabiri and Gharib (2005) determined that jet diameter changes during the jet ejection phase can contribute to higher ejection efficiency, i.e., a high impulse-to-energy-expended ratio, and higher F -values. Because the energetic cost of ejecting fluid in the form of an isolated vortex ring without a trailing jet is lower than that of a vortex ring with a trailing jet (Krueger 2001), squids employing *jet mode I* are operating close to the expected peak efficiency of pulsed fluid transport. Comparisons of propulsive efficiency of *jet modes I* and *II* are consistent with these findings and, in fact, provide the first evidence of this in a truly self-propelled setting. Squids using *jet mode II* produce higher overall thrust per jet pulse but have lower propulsive efficiency (lower impulse-to-energy-expended ratio) (Bartol et al., manuscript in preparation). In general, *jet mode II* was most prevalent at speeds >1.5 – 2.0 DMLs $^{-1}$ and in larger adult *L. brevis* when the highest thrusts were required, although there was no obvious, abrupt shift in jet modes for juvenile/adults, either as a function of speed or size. In fact, there were many sequences when *L. brevis* switched between the two modes while swimming at a constant speed.

The propulsive efficiencies for *jet mode I* (mean = 80.7%) and *jet mode II* (71.3%) for *L. brevis* juveniles and adults (2.0–8.5 cm DML) were lower than those reported by Anderson and Grosenbaugh (2005) for adult *D. pealeii* (27 cm DML), which exhibited a mean propulsive efficiency of 86% for speeds above 0.65 DMLs $^{-1}$ and 93% for speeds above 1.6 DMLs $^{-1}$. Although efficiencies

were calculated differently in the present study, Anderson’s and Grosenbaugh’s (2005) findings suggest that elongated jets can also have high propulsive efficiencies, just as shorter isolated vortex ring jets. Anderson and Grosenbaugh (2005) felt that the increase in η_p with swimming speed that they found was a product of reduced slip, i.e., the ratio by which the average jet velocity exceeds the swimming speed.

Selection of jet mode seems to correlate with fin activity, although additional jet and fin data are clearly needed to fully corroborate this. When *jet mode I* was used most heavily, high fin activity was often observed, whereas when *jet mode II* was used most heavily (high speeds), fin activity was generally low. This seems reasonable, given the discrepancy in magnitude of impulse between the two jet modes; *jet mode I* produces low thrust relative to *jet mode II* and thus augmentation by fin thrust may be required to maintain swimming speed. Augmentation by fin force is beneficial because fins produce thrust by imparting relatively small accelerations to relatively large masses of water and thus have high propulsive efficiency (Alexander 1968; Lighthill 1970). Our data support this, with higher propulsive efficiency being detected for fins versus the jet. Coupling *jet mode I* with high fin activity should lead to a high overall propulsive efficiency, which was also consistent with our limited dataset. In the present study, the highest combination of *jet mode I* and high fin activity occurred at speeds between 0.5 and 2.0 DML s $^{-1}$, which is close to the range in speed at which oxygen consumption is lowest in *L. brevis* (Bartol et al. 2001a).

Juvenile and adult *L. brevis* exhibit a wide diversity of fin motions, from more wave-like (undulatory) motions to more flap-like motions (Bartol et al. 2001b; Hoar et al. 1994). Consequently, it is not surprising that a multitude of fin wake patterns were observed. The two most prominent patterns for tail-first swimming involved well-defined, consistent vortex structures; in *fin mode I* a coherent vortex ring was shed with each half stroke, while in *fin mode II*, the upstroke and downstroke vortex rings were seemingly linked in a more complex vortex structure. In *fin mode II*, the downstroke’s leading-edge vortex served as the subsequent upstroke’s trailing-edge vortex, which could potentially accelerate upstroke vortex development and augment circulation, as is the case for insect wings (Birch and Dickinson 2003). This augmentation of circulation could lead to enhanced production of force. The data presented here are insufficient to either correlate propulsive efficiency with fin wake mode or even to

determine if the two observed modes represent fundamentally different hydrodynamic “gaits.” These are areas that merit further study.

Caveats and concluding thoughts

A number of factors make estimating propulsive efficiency in squids throughout ontogeny challenging. First, as mentioned previously, paralarvae have a very different ecology than do juveniles and adults and reside in an intermediate Re regime with unique fluid constraints. Because paralarvae swim predominantly along a vertical axis, paralarval displacement over a full jet cycle is strongly dependent on the refill duration and concomitant sinking, which can be highly variable. To account for this, only propulsive efficiency during the exhalant jet phase was considered. The different resident flow regimes of paralarvae and juveniles/adults along with their accompanying fluid constraints pose unique problems for analysis of propulsive efficiency as well. The relatively higher viscosity environment of paralarvae will dissipate jet kinetic energy rapidly, which will contribute to artificially high values of propulsive efficiency when impulse and kinetic energy are used in calculations. Within this intermediate Re regime, paralarvae experience higher relative viscous drag than do juveniles and adults, and these high drag terms can have a significant impact on calculations of propulsive efficiency by modifying the relationship between thrust and displacement (which were approximated as essentially independent in this study).

The refill phase has not been considered directly in the present analyses. Refill is an important consideration for analyses based on measurements of momentum where thrust is determined as the rate at which the inlet momentum is changed at the outlet. For pulsatile jets, an analysis of momentum is further complicated by the influence of unsteady pressure effects (i.e., pressure at the inlet and outlet cannot be ignored). In the present study, these issues were avoided by using a vorticity-based approach. Specifically, the hydrodynamic impulse in equation (1) is computed from the vorticity field and is equal to the impulse (integral of force in time) required to generate the flow (Lamb 1932; Saffman 1992). It follows that the force required to generate the flow is equal to the rate at which hydrodynamic impulse is added to the flow, which is in turn related to the rate at which vorticity is added to the flow through equation (1). The equality between force and rate of addition of hydrodynamic impulse holds for both steady and unsteady flows. In the present study, the

upstream flow was non-vortical, so only downstream vorticity was relevant for computing thrust. In the case of the jet, only the jet vorticity was related to the thrust generated by jetting and the refill process did not need to be explicitly included. All forces were, however, computed as averages over time using I/T where T was the relevant period (e.g., duration of jet exhalation or propulsive cycle period); time-varying force was not considered.

The role of the fins and their interaction with the jet adds another layer of complexity to calculations of propulsive efficiency. Although the fins have been largely overlooked in some previous locomotive studies of squids (Johnson et al. 1972; O’Dor 1988; Anderson and DeMont 2000; Anderson and Grosenbaugh 2005) with the studies of Hoar et al. (1994), Bartol et al. (2001a, 2001b), and Anderson and DeMont (2005) being notable exceptions, the present study, which together with Stewart et al. (in review) represent the first DPIV studies on squid fins, demonstrates that fins can contribute significantly to the production of locomotive force and improve propulsive efficiency (overall propulsive efficiencies were 0.8–10.2% greater than jet propulsive efficiencies). Like the jet, the fins produce multiple wake modes, but the effects of these various fin modes on propulsive efficiency are not well understood. Identifying those combinations of jet/fin wake modes that most affect propulsive efficiency is a critical step in understanding the dual locomotive system of squids. Not only will an integrated fin/jet approach provide a more comprehensive assessment of true propulsive efficiency, but it will also help in the identification of interconnected fin/jet gaits.

Quantifying the synergistic effects of the jet and fins of squid is no trivial undertaking. Conventional planar, stereo, and even scanning DPIV lack sufficient spatial resolution to simultaneously visualize and quantify the complex vortex-wake flows around the fins and jet. Consequently, more powerful 3D approaches, such as defocusing DPIV (Pereira and Gharib 2002, 2004; Kajitani and Dabiri 2005; Pereira et al. 2006) that provides volumetric, three-component velocity field data, will be necessary to fully understand the interdependence of the jet and fins. As stressed by Lauder and Tytell (2006), these approaches to the quantification of flow should be coupled with high-speed, high-resolution videography for accurate measurements of kinematics. Not only will a full 3D approach allow for simultaneous quantification of jet and fin flows, but it will also improve overall calculations of impulse/force because assumptions of axisymmetry will not be necessary. The technical challenges of applying these approaches

are certainly significant, but this research holds much promise for understanding swimming performance in a very unique, highly flexible, dual-mode locomotive system.

Acknowledgments

We thank Rick Blob and Gabe Rivera for organizing the symposium and for inviting us. Many thanks to A Woolard, J Brown, K Spangler, C Morgan, and K Parker for assistance during collection and processing of data and Ty Hedrick for the use of his Matlab digitization program. We gratefully acknowledge field assistance from the Virginia Institute of Marine Science's Eastern Shore Laboratory. The research was funded by the National Science Foundation (IOS 0446229 to I.K.B., P.S.K., and J.T.T.) and the Thomas F. Jeffress and Kate Miller Jeffress Memorial Trust (J-852 to I.K.B.).

References

- Alexander RM. 1968. Animal mechanics. Seattle: University of Washington Press.
- Alexander RM. 1977. Swimming. In: Alexander RM, Goldspink G, editors. Mechanics and energetics of animal locomotion. London: Chapman and Hall. p. 222–48.
- Anderson EJ, DeMont ME. 2000. The mechanics of locomotion in the squid *Loligo pealei*: locomotory function and unsteady hydrodynamics of the jet and intramantle pressure. *J Exp Biol* 203:2851–63.
- Anderson EJ, DeMont ME. 2005. The locomotory function of the fins in the squid *Loligo pealei*. *Mar Fresh Behav Phys* 38:169–89.
- Anderson EJ, Grosenbaugh MA. 2005. Jet flow in steadily swimming adult squid. *J Exp Biol* 208:1125–46.
- Bartol IK, Mann R, Patterson MR. 2001a. Aerobic respiratory costs of swimming in the negatively buoyant brief squid *Lolliguncula brevis*. *J Exp Biol* 204:3639–53.
- Bartol IK, Patterson MR, Mann R. 2001b. Swimming mechanics and behavior of the negatively buoyant shallow-water brief squid *Lolliguncula brevis*. *J Exp Biol* 204:3655–82.
- Birch JM, Dickinson MH. 2003. The influence of wing-wake interactions on the production of aerodynamic forces in flapping flight. *J Exp Biol* 206:2257–72.
- Boletzky SV. 1974. The “larvae” of cephalopoda: a review. *Thalassia Jugosl* 10:45–76.
- Boletzky SV. 1987. Embryonic phase. In: Boyle PR, editor. Cephalopod life cycles, Vol. II. London: Academic Press. p. 5–31.
- Dabiri JO, Colin SP, Costello JH. 2006. Fast-swimming hydromedusae exploit velar kinematics to form an optimal vortex wake. *J Exp Biol* 209:2025–33.
- Dabiri JO, Colin SP, Costello JH, Gharib M. 2005. Flow patterns generated by oblate medusan jellyfish: field measurements and laboratory analyses. *J Exp Biol* 208:1257–65.
- Dabiri JO, Gharib M. 2005. Starting flow through nozzles with temporally variable exit diameter. *J Fluid Mech* 538:111–36.
- Fields WG. 1965. The structure, development, food relations, reproduction, and life history of the squid *Loligo opalescens* Berry. *Fish Bull Calif Fish Game* 131:1–108.
- Gharib M, Rambod E, Shariff K. 1998. A universal time scale for vortex ring formation. *J Fluid Mech* 360:121–40.
- Gilly WF, Hopkins B, Mackie GO. 1991. Development of giant motor axons and neural control of escape responses in squid embryos and hatchlings. *Biol Bull* 180:209–20.
- Gosline JM, DeMont ME. 1985. Jet-propelled swimming in squids. *Sci Am* 252:96–103.
- Hanlon RT, Hixon RF, Hulet WH. 1983. Survival, growth, and behavior of the loliginid squids *Loligo plei*, *Loligo pealei*, and *Lolliguncula brevis* (Mollusca: Cephalopoda) in closed sea water systems. *Biol Bull* 165:637–85.
- Hanlon RT, Messenger JB. 1996. Cephalopod behaviour. Cambridge: Cambridge University Press.
- Hoar JA, Sim E, Webber DM, O'Dor RK. 1994. The role of fins in the competition between squid and fish. In: Maddock L, Bone Q, Rayner JMC, editors. Mechanics and physiology of animal swimming. Cambridge: Cambridge University Press. p. 27–33.
- Holman JP. 2000. Experimental methods for engineers. 7th edition. New York: McGrall Hill.
- Johnson W, Soden PD, Trueman ER. 1972. A study in jet propulsion: an analysis of the motion of the squid, *Loligo vulgaris*. *J Exp Biol* 56:155–65.
- Kajitani L, Dabiri D. 2005. a full three-dimensional characterization of defocusing digital particle image velocimetry. *Meas Sci Tech* 16:790–804.
- Kier WM. 1988. The arrangement and function of molluscan muscle. In: Trueman ER, Clarke MR, Wilbur KM, editors. The mollusca, form and function. New York: Academic Press. p. 211–52.
- Kier WM. 1989. The fin musculature of cuttlefish and squid (Mollusca, Cephalopoda): morphology and mechanics. *J Zool* 217:23–38.
- Kier WM, Smith KK. 1985. Tongues, tentacles and trunks: the biomechanics of movement in muscular-hydrostats. *J Linn Soc Lond Zool* 83:307–24.
- Kier WM, van Leeuwen J. 1997. A kinematic analysis of tentacle extension in the squid *Loligo pealei*. *J Exp Biol* 200:41–53.
- Krueger PS. 2001. The significance of vortex ring formation and nozzle exit over-pressure to pulsatile jet propulsion. PhD Thesis. Pasadena, CA: California Institute of Technology.
- Krueger PS, Gharib M. 2003. The significance of vortex ring formation to the impulse and thrust of a starting jet. *Phys Fluid* 15:1271–81.
- Krueger PS, Gharib M. 2005. Thrust augmentation and vortex ring evolution in a fully-pulsed jet. *AIAA J* 43:792–801.
- Lamb H. 1932. Hydrodynamics. New York: Dover.

- Lauder GV, Tytell ED. 2006. Hydrodynamics of undulatory propulsion. In: Shadwick RE, Lauder GV, editors. Fish biomechanics, fish physiology series, Vol. 23. p. 425–68.
- Lighthill MJ. 1960. Note on the swimming of slender fish. *J Fluid Mech* 9:305–17.
- Lighthill MJ. 1970. Aquatic animal propulsion of high hydromechanical efficiency. *J Fluid Mech* 44:265–301.
- Okutani T. 1987. Juvenile morphology. In: Boyle PR, editor. Cephalopod life cycles, Vol. II. Florida: Associated Press.
- O'Dor RK. 1988. Forces acting on swimming squid. *J Exp Biol* 137:421–42.
- O'Dor RK, Balch N, Foy EA, Helm PL. 1986. The locomotion and energetics of hatchling squid, *Illex illecebrosus*. *Am Mal Bull* 4:55–60.
- O'Dor RK, Webber DM. 1986. The constraints on cephalopods: why squid aren't fish. *Can J Zool* 64:1591–605.
- Packard A. 1969. Jet propulsion and the giant fibre response of *Loligo*. *Nature* 221:875–7.
- Pereira F, Gharib M. 2002. Defocusing digital particle image velocimetry and the three-dimensional characterization of two-phase flows. *Meas Sci Techn* 13:683–94.
- Pereira F, Gharib M. 2004. A method for three-dimensional particle sizing in two-phase flows. *Meas Sci Techn* 15:2029–38.
- Pereira F, Stüer H, Graff EC, Gharib M. 2006. Two-frame 3d particle tracking. *Meas Sci Techn* 17:1680–92.
- Prandtl L. 1952. Essentials of fluid dynamics. London: Blackie and Son, Ltd.
- Preuss T, Lebaric ZN, Gilly WF. 1997. Post-hatching development of circular mantle muscles in the squid *Loligo opalescens*. *Biol Bull* 192:375–87.
- Saffman PG. 1992. Vortex dynamics. Cambridge: Cambridge University Press.
- Sidie J, Holloway B. 1999. Geotaxis in the squid hatchling *Loligo pealei*. *Am Zool* 39:74A.
- Sweeney MJ, Roper CFE, Mangold K. 1992. “Larval” and juvenile cephalopods: a manual for their identification. *Smithson Contrib Zool* 513:1–282.
- Thompson JT, Kier WM. 2001a. Ontogenetic changes in mantle kinematics during escape-jet locomotion in the oval squid, *Sepioteuthis lessoniana* Lesson, 1830. *Biol Bull* 201:154–66.
- Thompson JT, Kier WM. 2001b. Ontogenetic changes in fibrous connective tissue organization in the oval squid, *Sepioteuthis lessoniana* Lesson, 1830. *Biol Bull* 201:136–53.
- Thompson JT, Kier WM. 2002. Ontogeny of squid mantle function: changes in the mechanics of escape-jet locomotion in the oval squid, *Sepioteuthis lessoniana* Lesson, 1830. *Biol Bull* 203:14–26.
- Thompson JT, Kier WM. 2006. Ontogeny of mantle musculature and implications for jet locomotion in oval squid *Sepioteuthis lessoniana*. *J Exp Biol* 209:433–43.
- Vecchione M, Roper CFE. 1991. Cephalopods observed from submersibles in the western North Atlantic. *Bull Mar Sci* 49:433–45.
- Vecchione M, Roper CFE, Widder EA, Frank TM. 2002. In situ observations on three species of large-finned deep-sea squids. *Bull Mar Sci* 71:893–901.
- Vecchione M, Shea E, Bussarawit S, Anderson F, Alexeyev D, Lu C-C, Okutani T, Roeleveld M, Chotiyaputta C, Roper C, Jorgensen E, Sukramongkol N. 2005. Systematic of Indo-West Pacific loliginids. *Phuket Mar Biol Cent Res Bull* 66:23–6.
- Vecchione M, Young RE, Guerra A, Lindsay DJ, Clague DA, Bernhard JM, Sager WW, Gonzalez AF, Rocha FJ, Segonzac M. 2001. Worldwide observations of remarkable deep-sea squids. *Science* 294:2505–6.
- Vogel S. 1987. Flow-assisted mantle cavity refilling in jetting squid. *Biol Bull* 172:61–8.
- Vogel S. 1994. Life in moving fluids; the physical biology of flow. 2nd edition. Princeton, NJ: Princeton University Press.
- Vogel S. 2003. Comparative biomechanics: life's physical world. Princeton: Princeton University Press.
- Ward DV, Wainwright SA. 1972. Locomotory aspects of squid mantle structure. *J Zool Lond* 167:437–49.
- Weihls D. 1974. Energetic advantages of burst swimming of fish. *J Theor Biol* 48:215–29.
- Westerweel J, Dabiri D, Gharib M. 1997. The effect of a discrete window offset on the accuracy of cross-correlation analysis of digital PIV recordings. *Exp Fluids* 23:20.
- Willert CE, Gharib M. 1991. Digital particle image velocimetry. *Exp Fluids* 10:181–93.
- Young RE, Harman RF. 1988. “Larva”, “paralarva”, and “sub-adult” in cephalopod terminology. *Malacologia* 29:201–7.
- Zeidberg LD, Hamner WM. 2002. Distribution of squid paralarvae, *Loligo opalescens* (Cephalopoda: Myopsida), in the Southern California Bight in the three years following the 1997–1998 El Niño. *Mar Biol* 141:111–22.